Electron Density Studies of Porphyrins and Phthalocyanines. 5. Electronic Ground State of Iron(II) Tetraphenylporphyrin Bis(tetrahydrofuran)

C. Lecomte,*† R. H. Blessing,‡ P. Coppens,* and A. Tabard§

Contribution from the Department of Chemistry, State University of New York at Buffalo, Buffalo, New York 14214. *Received April 4, 1986*

Abstract: The electron density in iron(II) tetraphenylporphyrin bis(tetrahydrofuran) has been derived from low-temperature (100 K) X-ray diffraction data. At 100 K, the cell dimensions are a = 11.039 (4) Å, b = 11.734 (6) Å, c = 9.540 (3) Å, α = 103.90 (5)°, β = 114.71 (4)°, and γ = 102.82 (4)° in space group $P\bar{1}$. On cooling of the crystal from room temperature to 100 K, the axial Fe–O distance contracts from 2.351 (3) to 2.2922 (7) Å, while the Fe–N distances increase from 2.057 (3) to 2.067 (1) Å. Magnetic measurements indicate that no magnetic transition is associated with the Fe–O contraction. The electron density maps and the quantitative least-squares analysis support the $^5E_{2g}$ state as the leading contributor to the ground state of the complex. Experimental d-electron populations are $d_{xy}^{0.93}$, $d_{xz,yz}^{2.52}$, $d_{z^2}^{0.88}$, and $d_{x^2-y^2}^{1.42}$. When compared with the $^5E_{2g}$ state, these populations give evidence for the effects of σ-donation and π-back-bonding.

The proper description of the electronic ground state of iron porphyrins and its dependence on coordination changes is of considerable importance for our understanding of the biological action of heme proteins. As part of a program to map the electron distribution in hemoglobin model compounds, we have studied a series of complexes including $Co^{II}TPP$ (TPP = tetraphenylporphyrin),[1] $Fe^{III}OMeTPP$ (OMe = methoxy),[2] $Fe^{II}Pc$ (Pc = phthalocyanine),[3] and $Fe^{II}TPP$.[4] While the electron density in the tetraphenylporphyrin ring appears rather invariant, large differences are observed around the transition-metal atoms. As may be expected, the distributions differ for low-spin (CoTPP), high-spin (FeOMeTPP), and intermediate-spin (FePc, FeTPP) complexes. In addition, the experiment allows distinction between contenders for the leading contributing configuration to the electronic ground state, as the different configurations may correspond to very different spatial distributions, even when closely spaced in energy.[3]

In general, nonzero electron populations are obtained for the crystal field destabilized orbitals. This indicates that the simplified ionic picture is inadequate, as may be expected, and that covalency (σ-donation) plays an important role in the metal–ligand interaction. However, comparison of the distribution in CoTPP[1] with the polarized neutron results on CoPc[5] confirms that mixing of excited configurations is also important.[6]

The axial ligands in $Fe^{II}(THF)_2TPP$ are weakly bound. The solid slowly looses THF on standing, and in a THF-containing solution in benzene the iron appears five-coordinate.[7] Nevertheless, it is remarkable that the complex is high spin[7] and not in an intermediate triplet state like $Fe^{II}TPP$ or a low-spin state like $Fe^{II}(py)_2TPP$ (py = pyridine).[9] The room-temperature structure analysis by Reed et al.[7] has shown that the Fe(II) atom is rigorously centered in the porphyrin plane, thereby causing a greater radial core expansion than observed in any other iron porphyrin. We report here on the experimental electron density of the complex and the ground-state configuration that most closely describes the experimental results. No theoretical study on this complex has as yet been reported, but an ab initio SCF calculation has now been initiated.[10]

Experimental Section

Data Collection. Two crystals were used for low-temperature data collection on an Enraf-Nonius CAD4F diffractometer. The gas-stream temperature was maintained at 100 K to within ±2 K as monitored by a copper–constantan thermocouple. Unit cell dimensions were obtained by least-squares fit to the observed setting angles of the $K\alpha_1$ peaks of 21 centered reflections with θ greater than 15°. Crystal data and experimental conditions are given in Table I. The full-step scan profile of each

Table I. Crystal Data and Experimental Conditions

$Fe(TPP)(THF)_2$	$C_{52}H_{44}N_4O_2Fe$
M_r	812.45
space group	$P\bar{1}$
cell dimens	
$a/b/c$, Å	
100 K	11.039 (4)/11.734 (6)/9.530 (3)
rt[a]	11.354 (3)/11.804 (3)/9.688 (3)
$\alpha/\beta/\gamma$, deg	
100 K	103.90 (5)/114.71 (4)/102.82 (4)
rt[a]	103.92 (2)/115.9 (3)/102.38 (2)
Z	1
d_{calcd}, mg mm^{-3}	1.332
abs coeff, mm^{-1}	0.4161
no. of cryst used for data collcn	2

	cryst	cryst 2
cryst dimens, mm	0.3 × 0.15 × 0.4	0.2 × 0.4 × 0.7
mounted approximately parallel to	[0,0,1]	[0,0,1]
capillary diam, mm	0.36	0.46
wall thickness, mm	0.016	0.016
abs coeff, mm^{-1}	1.058	1.058
diffractometer	CAD4F	
radiation (λ, Å)	Mo Kα (0.709 30)	
θ_{min}–θ_{max}	2–33	2–60
$(\sin\theta)/\lambda_{max}$	0.66	1.20
no. of reflcns measd	11 610	9490
no. of std reflcns	8	6
ψ scans	yes	yes
scan type	ω–2θ	
scan width	$1 + 0.34 \tan\theta$	
scan speed, deg/min	4–0.33	
detector aperture	9	9
takeoff angle, deg	3	3
hkl limits	$-14 < h < 15$; $-17 < k < 17$; $0 < l < 14$	$-23 < h < 20$; $-28 < k < 26$; $0 < l < 20$
no. of unique reflcns	7539	7384

[a] From ref 7.

† Permanent address: Laboratoire de Cristallographie, Faculte des Sciences, Universite de Nancy I, 54506 Vandoeuvre Cedex, France.
‡ Permanent address: Medical Foundation of Buffalo, Buffalo, NY 14203.
§ Permanent address: Laboratoire de Chimie de Heterocycles, Faculte des Sciences Gabriel, 21000 Dijon, France.

(1) Stevens, E. D. *J. Am. Chem. Soc.* **1981**, *103*, 5087–5095.
(2) Lecomte, C.; Chadwick, D. L.; Coppens, P.; Stevens, E. D. *Inorg. Chem.* **1983**, *22*, 2982–2992.
(3) Coppens, P.; Li, L. *J. Chem. Phys.* **1984**, *81*, 1983–1993.
(4) Tanaka, K.; Elkaim, E.; Li, L.; Zhu, N. J.; Coppens, P. *J. Chem. Phys.* **1986**, *84*, 6969–6978.
(5) Williams, G.; Figgis, B. N.; Mason, R. *J. Chem. Soc. Dalton* **1981**, 734–742.
(6) Coppens, P.; Holladay, A.; Stevens, E. D. *J. Am. Chem. Soc.* **1982**, *104*, 3546.

0002-7863/86/1508-6942$01.50/0

Table II. Range of Intensity Corrections (Gaussian Grid 4 × 8 × 16)

	cryst 1		cryst 2	
	min	max	min	max
cryst	0.870	0.943	0.808	0.927
capillary	0.940	0.965	0.809	0.965
beam profile	0.938	0.973	0.925	0.971
total	0.800	0.873	0.679	0.855
abs weighted path length, mm	0.151	0.365	0.197	0.562

Table III. Data Averaging

	cryst 1	cryst 2
no. of reflcns measd	11610	9490
agreement indices for averaging $R = \sum\|I - \bar{I}\|/\sum I$	0.023	0.018
no. of symmetry-independent reflcns	7539	7384
no. of symmetry-independent reflcns in combined data set	10333 (7088 with $I > 2\sigma_I$)	

reflection was recorded. To check the absorption corrections, several reflections were collected at a number of different ψ values. After completion of a least-squares refinement against the low-order data ($(\sin\theta)/\lambda < 0.75$ Å^{-1}), high-order reflections were calculated and those with an expected intensity greater than 5σ were measured up to $(\sin\theta)/\lambda = 1.2$ Å^{-1}. A total of 21 100 reflections were measured.

Data Processing. The data were processed with a new set of programs written by Blessing.[11] They include application of the Lehmann–Larsen formalism[12] to obtain peak–background boundaries for the strong reflections. Analytical functions are fitted to the peak widths of the strong reflections and subsequently applied to select the peak/background boundaries of the weaker intensity profiles. The treatment improves the reliability of the intensity estimates for the weak reflections for which the Lehmann–Larsen method often yields unreliable peak boundaries. Background substraction was based on a least-squares line fitted to the scan profile outside the calculated peak limits.

Cubic polynomials, least squares fitted to intensities of the standard reflections, showed a decline of about 20% for crystal 1 (this crystal was replaced at that time) and of about 4% for crystal 2. The instrumental instability factor defined by

$$P = \{[\sum\Delta^2(I) - \sum\sigma^2(I_o)]/\sum I_o^2\}^{1/2}$$

(where the sum is over the standard reflections) was estimated to be $P = 0.015$ and $P = 0.014$ for crystals 1 and 2, respectively. Here I_o is the intensity corrected for Lorentz polarization effects, $\Delta = I_o - I_c(t)$, $I_c(t)$ is calculated from the time-dependent scaling polynomials, and $\sigma(I_o)$ is the standard deviation due to counting statistics.

By using a numerical Gaussian integration method, we applied corrections for absorption by both the crystals and the capillaries and for inhomogeneity of the incident beam. The values of the transmission factors given in Table II show the importance of the capillary and beam profile corrections. The results of the data averaging are given in Table III. Error estimates $\sigma(I)$ include contributions from a variety of effects, including the Poisson variance of the count rates, the reproducibility of the scan angle positioning, the variances and covariances of the parameters of the straight line fitted to the background of the peak profile, errors in the time-dependent scaling polynomials, and the instrumental instability variance as defined above.[13]

Structure Refinement. Conventional Refinements. Starting parameters for a conventional refinement using low-order data ($(\sin\theta)/\lambda < 0.75$ Å^{-1}) were taken from ref 7. Scattering factors, including those for anomalous scattering of Fe, C, and N, were taken from ref 14, except for hydrogen,

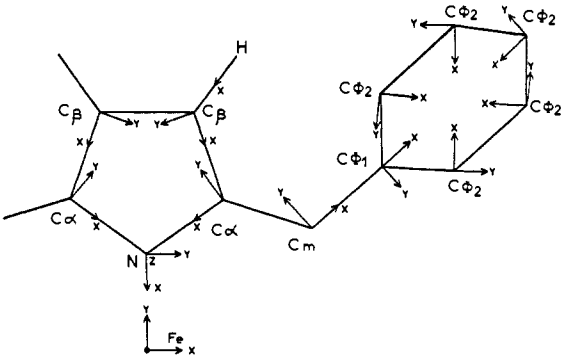

Figure 1. Definition of local coordinate systems used in the multipole refinement.

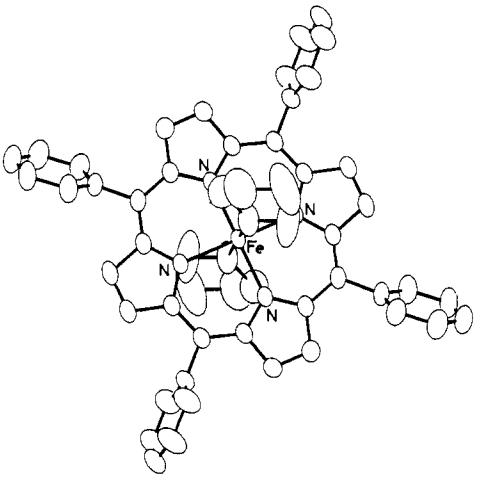

Figure 2. ORTEP drawing of the molecule. Ellipsoids are 50% probability surfaces.

for which the contracted scattering factor of Stewart, Davidson, and Simpson[15] was used. After a number of cycles all hydrogen atoms were located and included in the refinement. To obtain parameters unbiased by the spherical-atom assumption, all non-hydrogen parameters were subsequently varied in a high-order refinement ($0.75 < (\sin\theta)/\lambda < 1.20$ Å^{-1}). Both refinements give large thermal parameters for the carbon atoms of the THF ligand. Difference maps show a peak of 0.95 e/Å^3 close to the C(25) atom, which indicates a positional disorder. The peak was included in the refinement as a carbon atom with variable occupancy, constrained to equal the deficiency at the major C(25) position. The occupancy of the minor site converged at 0.157 (8); as a result the thermal parameters of C(25) decreased. It was not possible to refine a similar disorder for the C(26) atom. Final agreement factors are given in Table IV.

Charge Density Analysis. Multipole Refinement. In the model used,[16] the electron density at each atom is described by an expansion of atom-centered deformation functions:

$$\rho_{at}(r) = \rho_{core}(r) + P_{val}\rho_{valence}(\kappa r) + \sum_{l=0}^{4} R(\kappa' r) \sum_{m=-1}^{+l} P_{lm} y_{lm}(\mathbf{r}/r)$$

where ρ_{core} and $\rho_{valence}$ are spherical Hartree–Fock core and valence densities and y_{lm} represents spherical harmonic angular functions in real form. Slater-type radial functions of the form $R_{lm}(r) = Nr^{n(l)} \exp(-\kappa'\zeta r)$ were selected for the deformation functions of the carbon, nitrogen, oxygen, and hydrogen atoms; here N is a normalization parameter and n and ζ are chosen as described previously;[16] the κ's are refinable expansion–contraction parameters. As a single Slater-type function is not a good representation of the radial part of the d-electron density, Hartree–Fock radial functions, modified by a κ parameter, were used for the valence and deformation functions of the iron atom. The corresponding Fourier–Bessel transforms $\langle j_0\rangle$, $\langle j_2\rangle$, and $\langle j_4\rangle$ were taken from ref 14.

To reduce the number of variables to be refined, chemical symmetry was imposed on the molecule. This constraint was justified a posteriori

(7) Reed, C. A.; Mashiko, T.; Scheidt, W. R.; Spartalian, K.; Lang, G. *J. Am. Chem. Soc.* **1980**, *102*, 2302–2306.
(8) Boso, B.; Lang, G.; Reed, C. A. *J. Chem. Phys.* **1983**, *78*, 2561–2567.
(9) Kobayashi, H.; Yanagawa, Y. *Bull. Chem. Soc. Jpn.* **1972**, *45*, 450–456.
(10) Rohmer, M. M., private communication.
(11) Blessing, R. H. *Crystallogr. Rev.*, in press. Blessing, R. H. *J. Appl. Crystallogr.*, in press.
(12) Lehmann, M. S.; Larsen, F. K. *Acta Crystallogr., Sect. A: Cryst. Phys., Diffr., Theor. Gen. Crystallogr.* **1974**, *A30*, 580–584.
(13) McCandlish, L. E.; Stout, G. H.; Andrews, L. C. *Acta Crystallogr., Sect. A: Cryst. Phys., Diffr., Theor. Gen. Crystallogr.* **1975**, *A31*, 245–249.
(14) *International Tables for X-ray Crystallography*; Kynoch: Birmingham, England, 1974; Vol. 4.
(15) Stewart, R. F.; Davidson, E. R.; Simpson, W. T. *J. Chem. Phys.* **1965**, *42*, 3175–3187.
(16) Hansen, N. K.; Coppens, P. *Acta Crystallogr., Sect. A: Cryst. Phys., Diffr., Theor. Gen. Crystallogr.* **1974**, *A34*, 909–921.

Table IV. Summary of Least-Squares Results

description	I spherical atom	II spherical atom	III aspherical atom	IV aspherical atom
$(\sin\theta)/\lambda$ range, A^{-1}	0–0.75	0.75–1.2	0–0.75	0–1.2
no. of observns	4893	2195	4893	7088
no. of params	268	268	171	268 + 171 = 439
$R(F)$, %	3.80	3.03	2.48	2.43
$R_w(F)$, ($w = 1/\sigma^2(F)$)	5.40	3.50	2.94	2.84
$R(F^2)$, %	5.94	5.36	3.61	3.55
$R_w(F^2)$, %	10.40	7.06	5.88	5.70
GOF	2.17	0.94	1.11	0.98
scale factor	*a*	0.3778 (2)	0.3808 (2)	0.3819 (2)

[a] This refinement was made with a different data processing routine and the scale factor cannot be compared.

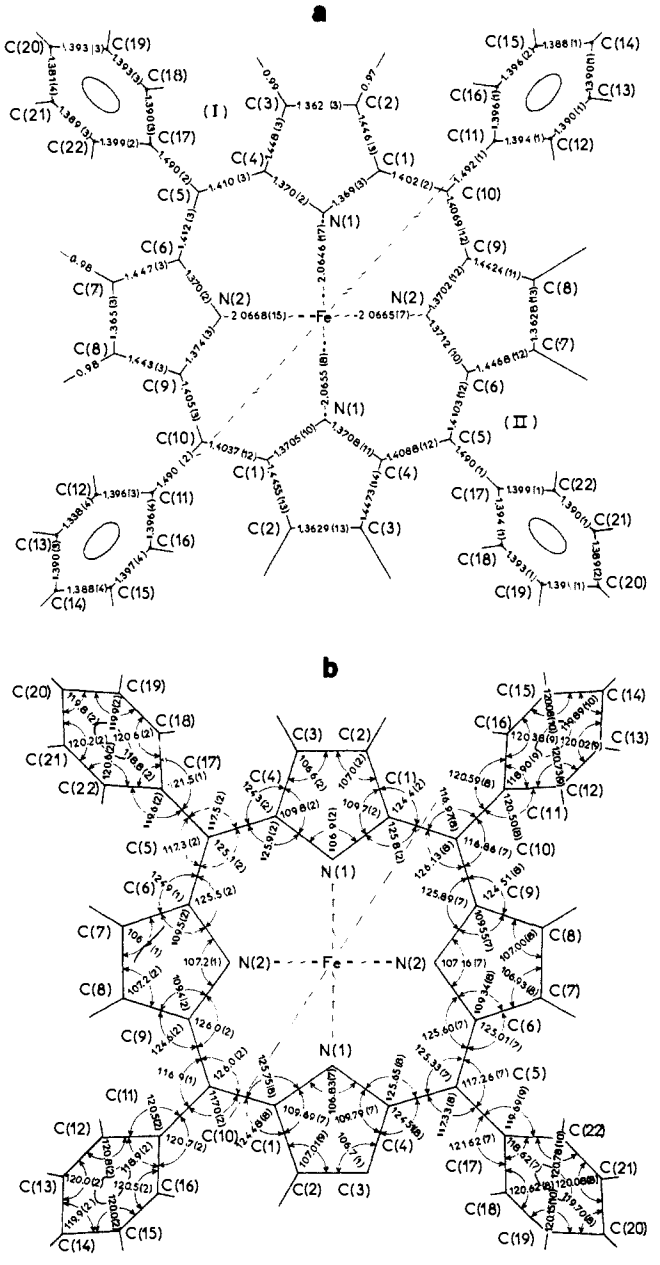

Figure 3. Bond distances (a) and angles (b). Upper left: high-order refinement. Lower right: multipole refinement.

by the lack of features in the residual maps, calculated after completion of the constrained refinement, and by a test refinement using crystallographic $\bar{1}$ symmetry, which did not lead to improved agreement between observed and calculated values. The iron atom was assumed to have D_{4h} symmetry, while the nitrogen, C_{meso}, and phenyl carbon atoms were constrained to have C_{2v} symmetry; C_s symmetry was assumed for the remaining carbon atoms in the pyrrole rings. No restrictions were imposed on the THF ligands. Chemically equivalent atoms in the porphyrin ring were constrained to have the same charge density parameters. The

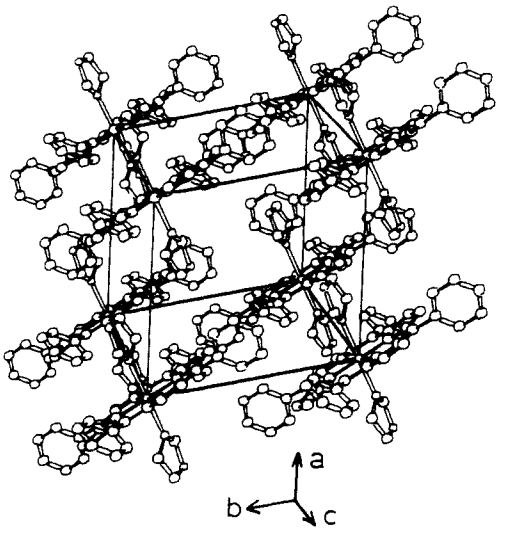

Figure 4. Packing diagram.

multipole expansion was truncated at the octopolar level ($l = 3$) for all carbon atoms, whereas hexadecapolar functions were included for Fe, O, and N. A single dipole along the C–H bond was used for all hydrogen atoms. The local coordinate systems are defined in Figure 1.

Two different multipole refinements are described here. The first (referred to as III) was restricted to reflections with $(\sin\theta)/\lambda < 0.75$ Å^{-1}; the thermal and positional parameters were fixed at the values from the high-order refinement. In the second multipole refinement (IV), all data were used and all structural parameters were refined along with charge density parameters. The least-squares results are summarized in Table IV. Tables V and VI give the fractional coordinates and the temperature factors. An ORTEP drawing of the molecule is shown in Figure 2, and parts a and b of Figures 3 give the bond distances and angles obtained with refinements II and IV. A packing diagram is shown in Figure 4.

Population parameters from refinements III and IV are listed in Table VII. Both refinements gave improved agreement factors when compared with the spherical-atom model (Table IV).

Deformation Maps. In order to illustrate the asymmetry of the atomic charge distribution, X–X deformation density maps were calculated. They are defined as

$$\rho_{X\text{-}X}(r) = \frac{2}{V}\sum_{H}(F_o/k - F_c)\exp(-2\pi i H\cdot r)$$

where the calculated amplitudes F_c are based on the parameters from the high-order refinement and F_o is given the sign of F_c.

Results and Discussion

Description of the Crystal Structure. Refinements II and IV both give very similar results for the geometry of the molecule, results of the latter being slightly more precise because of the larger number of observations. As the iron atom lies on an inversion center of the triclinic cell, it is located exactly in the plane of the four nitrogen atoms. The nitrogen–iron–oxygen angles are the same at low and room temperatures (N(1)–Fe–O = 93.00 (3) (100 K) and 92.9 (1)° (rt); N(2)–Fe–O = 87.12 (3) (100 K) and 87.1 (1)° (rt)). The distance to the axial ligand, however, changes considerably on cooling: Fe–O = 2.351 (3) Å at room temperature compared with 2.2922 (7) Å at 100 K; this contraction is accompanied by an increase of the Fe–N bond lengths (⟨Fe–N⟩ =

Table V. Fractional Coordinates and Standard Deviations[a]

atom	x/a	y/b	z/c
Fe	0	0	0
	0	0	0
N(1)	-0.01740 (18)	0.16657 (13)	0.10629 (17)
	-0.01733 (7)	0.16664 (6)	0.10649 (8)
N(2)	0.10172 (16)	-0.00869 (13)	0.23260 (17)
	0.10200 (7)	-0.00866 (6)	0.23254 (8)
C(1)	-0.09751 (19)	0.22588 (14)	0.02079 (20)
	-0.09753 (8)	0.22599 (7)	0.02087 (9)
C(2)	-0.11091 (22)	0.32204 (17)	0.13437 (23)
	-0.11097 (9)	0.32215 (7)	0.13438 (10)
C(3)	-0.03762 (23)	0.31989 (18)	0.28880 (21)
	-0.03781 (9)	0.31990 (8)	0.28884 (10)
C(4)	0.02079 (18)	0.22191 (15)	0.26992 (19)
	0.02081 (8)	0.22211 (7)	0.27015 (9)
C(5)	0.10042 (18)	0.18710 (14)	0.40095 (18)
	0.10039 (8)	0.18705 (7)	0.40075 (9)
C(6)	0.13950 (18)	0.08004 (14)	0.38144 (19)
	0.13917 (8)	0.07999 (7)	0.38137 (9)
C(7)	0.22979 (20)	0.04956 (16)	0.51689 (20)
	0.22967 (9)	0.04951 (7)	0.51661 (9)
C(8)	0.24592 (20)	-0.05775 (16)	0.44644 (20)
	0.24587 (9)	-0.05770 (7)	0.44655 (9)
C(9)	0.16711 (18)	-0.09293 (14)	0.26833 (19)
	0.16705 (8)	-0.09273 (7)	0.26854 (9)
C(10)	0.16353 (17)	-0.19504 (14)	0.15182 (18)
	0.16342 (8)	-0.19499 (7)	0.15191 (9)
C(11)	0.24140 (18)	-0.27526 (14)	0.21863 (20)
	0.24145 (8)	-0.27521 (7)	0.21897 (9)
C(12)	0.39009 (22)	-0.23521 (18)	0.29019 (29)
	0.38993 (9)	-0.23529 (8)	0.28992 (11)
C(13)	0.46327 (24)	-0.30961 (21)	0.35233 (30)
	0.46310 (9)	-0.30982 (8)	0.35213 (12)
C(14)	0.38847 (25)	-0.42553 (20)	0.34406 (25)
	0.38826 (10)	-0.42557 (9)	0.34412 (11)
C(15)	0.24064 (29)	-0.46633 (23)	0.27444 (35)
	0.24056 (10)	-0.46608 (9)	0.27495 (13)
C(16)	0.16728 (23)	-0.39124 (19)	0.21222 (30)
	0.16715 (9)	-0.39114 (8)	0.21255 (12)
C(17)	0.15394 (19)	0.27341 (16)	0.57421 (19)
	0.15400 (8)	0.27340 (7)	0.57402 (9)
C(18)	0.11690 (22)	0.23227 (18)	0.68090 (22)
	0.11700 (9)	0.23249 (8)	0.68135 (10)
C(19)	0.17538 (28)	0.31204 (23)	0.84570 (23)
	0.17560 (10)	0.31250 (9)	0.84602 (11)
C(20)	0.27248 (30)	0.43398 (22)	0.90502 (24)
	0.27290 (11)	0.43418 (9)	0.90557 (11)
C(21)	0.30842 (29)	0.47624 (18)	0.79928 (27)
	0.30897 (10)	0.47649 (8)	0.79915 (11)
C(22)	0.24898 (23)	0.39716 (16)	0.63449 (23)
	0.24893 (9)	0.39716 (8)	0.63428 (10)
C(23)	0.2763 (3)	0.0503 (3)	-0.0621 (4)
	0.2762 (1)	0.0501 (1)	-0.0620 (1)
C(24)	0.4245 (4)	0.1468 (4)	0.0094 (6)
	0.4246 (1)	0.1466 (1)	0.0095 (1)
C(25)	0.4783 (5)	0.1838 (8)	0.1914 (8)
	0.4779 (1)	0.1838 (2)	0.1915 (2)
C(25′)	0.456 (4)	0.249 (6)	0.191 (8)
C(26)	0.3409 (4)	0.1865 (5)	0.2025 (5)
	0.3411 (1)	0.1864 (1)	0.2023 (2)
O	0.22322 (20)	0.10095 (17)	0.04403 (21)
	0.22320 (7)	0.10096 (6)	0.04384 (8)

[a] Upper line = high-order refinement (II of Table IV). Lower line = full multipole refinement (IV of Table IV).

Table VI. Temperature Factors and Standard Deviations (Å^2 × 10^4)[a]

atom	U(11)	U(22)	U(33)	U(12)	U(13)	U(23)
Fe	147 (2)	109 (2)	88 (2)	70 (2)	46 (1)	44 (1)
	147 (1)	108 (1)	91 (1)	69 (1)	44 (1)	44 (1)
N(1)	172 (5)	121 (4)	95 (4)	78 (4)	48 (3)	45 (3)
	165 (2)	123 (2)	95 (2)	75 (2)	45 (2)	44 (2)
N(2)	157 (4)	117 (4)	94 (4)	68 (3)	47 (3)	43 (3)
	164 (3)	120 (2)	96 (2)	71 (2)	51 (2)	47 (2)
C(1)	163 (5)	117 (4)	111 (4)	71 (4)	50 (4)	47 (3)
	164 (3)	127 (3)	114 (3)	77 (3)	56 (2)	51 (2)
C(2)	218 (6)	154 (5)	137 (5)	117 (5)	72 (4)	58 (4)
	214 (3)	160 (3)	142 (3)	118 (3)	75 (3)	61 (2)
C(3)	218 (6)	173 (5)	129 (5)	118 (5)	79 (4)	55 (4)
	218 (3)	168 (3)	133 (3)	114 (3)	80 (3)	55 (2)
C(4)	165 (5)	124 (4)	105 (4)	74 (4)	55 (4)	44 (3)
	169 (3)	129 (3)	108 (3)	75 (2)	56 (2)	44 (2)
C(5)	166 (5)	125 (4)	97 (4)	64 (4)	54 (4)	37 (3)
	164 (3)	128 (3)	97 (2)	62 (2)	54 (2)	37 (2)
C(6)	155 (5)	113 (4)	99 (4)	57 (4)	48 (4)	41 (3)
	153 (3)	119 (3)	103 (3)	59 (2)	50 (2)	41 (2)
C(7)	179 (6)	151 (5)	104 (4)	76 (4)	43 (4)	51 (4)
	178 (3)	152 (3)	107 (3)	73 (2)	45 (2)	52 (2)
C(8)	190 (6)	153 (5)	107 (4)	90 (4)	48 (4)	58 (4)
	187 (3)	156 (3)	114 (3)	90 (3)	50 (2)	59 (2)
C(9)	158 (5)	120 (4)	109 (4)	67 (4)	47 (4)	47 (3)
	163 (3)	124 (3)	114 (3)	71 (2)	54 (2)	53 (2)
C(10)	152 (5)	122 (4)	113 (4)	67 (4)	50 (4)	49 (3)
	155 (3)	124 (3)	118 (3)	71 (2)	52 (2)	52 (2)
C(11)	145 (5)	115 (4)	130 (4)	65 (4)	45 (4)	56 (4)
	152 (3)	125 (3)	134 (3)	70 (2)	52 (2)	62 (2)
C(12)	153 (6)	158 (5)	244 (7)	69 (5)	52 (5)	74 (5)
	147 (3)	158 (3)	249 (4)	66 (3)	56 (3)	79 (3)
C(13)	166 (6)	209 (6)	230 (7)	101 (5)	31 (5)	73 (5)
	161 (3)	199 (3)	237 (4)	94 (3)	36 (3)	74 (3)
C(14)	233 (7)	215 (6)	176 (5)	138 (6)	69 (5)	109 (5)
	246 (4)	223 (4)	179 (3)	150 (3)	74 (3)	111 (3)
C(15)	260 (8)	218 (6)	303 (8)	136 (6)	148 (7)	189 (6)
	261 (4)	214 (4)	310 (4)	131 (3)	145 (4)	187 (3)
C(16)	192 (6)	182 (6)	271 (7)	90 (5)	110 (5)	141 (5)
	183 (3)	187 (3)	279 (4)	89 (3)	108 (3)	146 (3)
C(17)	163 (5)	134 (4)	97 (4)	60 (4)	62 (4)	33 (3)
	164 (3)	132 (3)	104 (3)	60 (2)	60 (2)	35 (2)
C(18)	196 (6)	177 (5)	135 (5)	58 (5)	87 (4)	55 (4)
	198 (3)	180 (3)	132 (3)	61 (3)	87 (3)	57 (3)
C(19)	277 (8)	253 (7)	124 (5)	129 (7)	105 (5)	65 (5)
	269 (4)	253 (4)	132 (3)	126 (3)	106 (3)	69 (3)
C(20)	297 (9)	200 (6)	126 (5)	116 (6)	61 (5)	17 (4)
	295 (4)	217 (4)	123 (3)	124 (3)	67 (3)	23 (3)
C(21)	275 (8)	139 (5)	173 (6)	51 (5)	72 (5)	9 (4)
	272 (4)	144 (3)	176 (3)	53 (3)	71 (3)	9 (3)
C(22)	217 (6)	126 (4)	154 (5)	46 (4)	89 (4)	36 (4)
	221 (3)	132 (3)	155 (3)	50 (3)	87 (3)	37 (2)
C(23)	241 (8)	239 (7)	295 (9)	79 (6)	174 (7)	107 (7)
	248 (4)	241 (4)	297 (5)	81 (3)	176 (4)	107 (4)
C(24)	225 (9)	375 (14)	381 (14)	71 (9)	170 (9)	177 (11)
	228 (4)	374 (5)	382 (6)	72 (4)	171 (4)	180 (5)
C(25)	191 (11)	558 (30)	347 (18)	2 (14)	23 (11)	243 (20)
	182 (5)	532 (8)	339 (7)	6 (5)	25 (5)	246 (12)
C(25′)	192 (30)					
C(26)	229 (9)	431 (17)	221 (9)	-59 (11)	63 (8)	-28 (10)
	235 (5)	411 (6)	217 (4)	-49 (4)	71 (4)	-24 (4)
O	182 (5)	208 (5)	167 (4)	39 (4)	82 (4)	59 (4)
	183 (3)	211 (3)	166 (3)	40 (2)	82 (2)	57 (2)

[a] Upper line = high-order refinement (II of Table IV). Lower line = full multipole refinement (IV of Table IV). The temperature factor expression is $T = \exp -2\pi^2(U_{11}h^2a^{*2} + U_{22}k^2b^{*2} + U_{33}l^2c^{*2} + 2U_{12}hka^*b^* + 2U_{13}hla^*c^* + 2U_{23}klb^*c^*)$.

2.057 (3) Å at room temperature[7] and 2.0665 (7) Å at 100 K. This pronounced temperature dependence is an indication of the shallowness of the Fe–O potential function and confirms the weakness of the axial bonding, at least at room temperature. To investigate whether the Fe–O contraction leads to an increase in the axial field strength sufficient to induce a high spin → low spin transition, the magnetic susceptibility of the complex was measured on a Foner magnetometer at the University of Nancy. The resulting magnetic moments, shown in Figure 5, indicate that the contraction is not sufficient to induce such a transition. In fact, at temperatures below that of the present X-ray study an *increase* in magnetic moment is obtained. The absence of a transition is in agreement with the Mössbauer results, which show a gradual shift of the quadrupole splitting toward more negative values on cooling.[8]

The THF ligands almost eclipse the C(5) meso carbon atoms; the dihedral angle between the mean plane of the THF molecule and that of C(5), Fe, O(1) is 11.8 (1)°. Although the THF ligand is disordered, the mean bond distances (O–C = 1.433 (8) Å and C–C = 1.523 (10) Å) are found to be equal within experimental

Table VII. Charge Density Parameters in $FeTPP(THF)_2$ and Comparison with FeTPP

		$FeTPP(THF)_2$ refinement III	$FeTPP(THF)_2$ refinement IV	FeTPP
metal	symmetry:	D_{4h}	D_{4h}	D_{4h}
κ		1.23 (5)	1.23 (5)	
κ' or $\zeta\kappa'$ ($bohr^{-1}$)		1.01 (2)	1.01 (1)	0.969 (17)
$P_{00}(4s)$		1.13 (14)	1.20 (12)	
P_{00}		5.94 (4)	5.92 (3)	7.18 (11)
P_{20}		−0.03 (2)	−0.02 (1)	0.43 (6)
P_{40}		−0.20 (5)	−0.09 (4)	−0.12 (6)
P_{44+}		0.09 (4)	0.16 (3)	−0.34 (7)
N	symmetry:	C_{2v}	C_{2v}	C_{2v}
n_l		2, 2, 2, 3, 4	2, 2, 3, 4	2, 2, 3, 4
κ		0.977 (3)	0.974 (2)	1.0 (2)
$\zeta\kappa'$		3.78 (1)	3.744 (8)	3.8 (not refined)
P_{val}		5.43 (3)	5.44 (3)	5.21 (17)
P_{11+}		0.05 (1)	0.06 (1)	0.13 (4)
P_{20}		0.02 (1)	0.01 (1)	*a*
P_{22+}		0.09 (1)	0.09 (1)	*a*
P_{31+}		−0.16 (2)	−0.15 (2)	*a*
P_{33+}		−0.02 (1)	−0.02 (1)	*a*
P_{40}		0.03 (2)	0.01 (2)	
P_{42+}		0.04 (2)	0.05 (2)	
P_{44+}		−0.01 (2)	−0.02 (2)	
C_α	symmetry:	C_s	C_s	C_s
n_l		2, 2, 3	2, 2, 3	2, 2, 3
κ		1.014 (3)	1.008 (3)	1.02 (2)
$\zeta\kappa'$		2.96	2.93 (1)	2.63 (16)
P_{val}		3.89 (3)	3.924 (3)	4.09 (19)
P_{11+}		−0.04 (1)	−0.04 (1)	0.02 (5)
P_{11-}		−0.01 (1)	−0.02 (1)	0.02 (5)
P_{20}		−0.15 (1)	−0.16 (1)	−0.23 (5)
P_{22+}		−0.01 (1)	−0.01 (1)	−0.04 (4)
P_{22-}		0.07 (1)	0.08 (1)	0.06 (6)
P_{31+}		0.03 (1)	0.03 (1)	0.00 (3)
P_{31-}		−0.01 (1)	−0.01 (1)	−0.02 (3)
P_{33+}		0.27 (2)	0.28 (1)	0.42 (7)
P_{33-}		0.05 (1)	0.05 (1)	0.06 (5)
C_β	symmetry:	C_s	C_s	C_s
n_l		2, 2, 3	2, 2, 3	2, 2, 3
κ		1.000 (3)	0.999 (3)	1.0 (1)
$\zeta\kappa'$		2.81	2.77	3.2 (not refined)
P_{val}		3.91 (4)	3.81 (3)	4.21 (9)
P_{11+}		0.03 (2)	0.03 (1)	0.04 (4)
P_{11-}		0.05 (2)	0.07 (2)	0.05 (3)
P_{20}		−0.19 (1)	−0.18 (1)	−0.14 (3)
P_{22+}		−0.02 (1)	−0.02 (1)	
P_{22-}		0.01 (1)	0.00 (1)	
P_{31+}		0.01 (1)	0.00 (1)	0.02 (3)
P_{31-}		0.02 (1)	0.02 (1)	0.02 (3)
P_{33+}		0.30 (1)	0.30 (1)	0.25 (3)
P_{33-}		0.10 (1)	0.10 (1)	0.08 (3)
C_m	symmetry:	C_{2v}	C_{2v}	C_s
n_l		2, 2, 3	2, 2, 3	2, 2, 3
κ		1.002 (8)	1.002 (3)	1.04 (3)
$\zeta\kappa'$		2.91	2.88	3.2 (not refined)
P_{val}		4.00 (4)	3.96 (4)	3.71 (28)
P_{11+}		0.02 (1)	0.01 (1)	0.03 (6)
P_{20}		−0.13 (2)	−0.17 (2)	*a*
P_{22+}		0.04 (1)	0.04 (1)	*a*
P_{31+}		−0.00 (1)	−0.01 (2)	*a*
P_{33+}		0.27 (2)	0.27 (2)	*a*
$C_{\phi 1}$	symmetry:	C_{2v}	C_{2v}	C_s
n_l		2, 2, 3	2, 2, 3	2, 2, 3
κ		0.999 (4)	0.996 (3)	1.0 (2)
$\zeta\kappa'$		2.97	2.93	2.65 (18)
P_{val}		3.39 (3)	3.99 (3)	4.52 (14)
P_{11+}		0.03 (2)	0.04 (1)	0.02 (5)
P_{20}		−0.19 (1)	−0.19 (1)	−0.37 (5)
P_{22+}		−0.01 (1)	−0.02 (1)	−0.03 (5)
P_{31+}		0.03 (2)	0.04 (2)	0.03 (4)
P_{33+}		−0.28 (2)	−0.30 (2)	−0.40 (6)

Table VII (Continued)

		FeTPP(THF)$_2$ refinement III	FeTPP(THF)$_2$ refinement IV	FeTPP
$C_{\phi 2}$	symmetry:	C_{2v}	C_{2v}	C_s
n_l		2, 2, 3	2, 2, 3	2, 2, 3
κ		1.011 (2)	1.007 (2)	1.016 (9)
ζ_κ'		2.93 (1)	2.92 (1)	3.2 (not refined)
P_{val}		3.87 (2)	3.86 (2)	4.22 (5)
P_{11+}		0.09 (2)	0.05 (1)	*a*
P_{20}		−0.20 (1)	−0.20 (1)	*a*
P_{22+}		−0.01 (1)	0.01 (1)	*a*
P_{31+}		0.01 (1)	0.00 (1)	*a*
P_{33+}		−0.28 (1)	−0.28 (1)	*a*
H_β	symmetry:	$C_{\infty v}$	$C_{\infty v}$	
n_l		1	1	
κ		1.05 (1)	1.00 (1)	
ζ_κ'		1.00	1.07 (3)	
P_{val}		1.16 (3)	1.13 (3)	
P_{10}		0.45 (5)	0.42 (5)	
$H_{\phi 2}$	symmetry:	$C_{\infty v}$	$C_{\infty v}$	
n_l		1	1	
κ		1.00 (2)	1.00 (1)	
ζ_κ'		1.00	1.11 (3)	
P_{val}		1.08 (2)	1.08 (9)	
P_{10}		0.28 (3)	0.27 (4)	

[a] Not comparable because of difference in coordinate system.

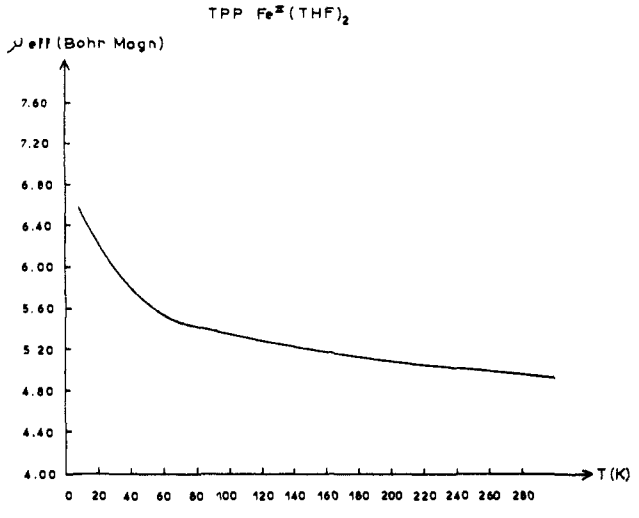

Figure 5. Temperature dependence of the magnetic moment as derived from susceptibility measurements.

errors to those of the THF molecule in the solid state[17] (O–C = 1.429 (6) Å, C–C = 1.511 (7) Å at 103 K) and in the gas phase[18] (O–C = 1.428 (1_5) Å, C–C = 1.536 (1_5) Å). Even though partial atoms could only be refined for C(25), the other THF carbon atoms had large U^{ij} values. The THF molecules are probably disordered among the two possible envelope and two possible half-chair conformations.

Comparison with the intermediate-spin complex FeTPP[4] shows some marked differences in geometry. In addition to the increase in the Fe–N distance, the C_α–N–C_α bond angle expands from 105.4 (1) to 107.0 (1)°, whereas C_α–C_m–C_α increases from 122.5 (2) to 125.6 (5)°, while the N–C_α–C_m bond angle remains constant. The nitrogen atoms are ±0.118 and ±0.145 Å from the mean porphinato plane compared to a displacement of only 0.035 Å in FeTPP. The distances of the iron atom from the pyrrole mean planes are ±0.385 Å and ±0.274 Å for the planes defined by N(1), C(1), C(2), C(3), C(4) and N(2), C(6), C(7), C(8), C(9), respectively.

Thermal Motion. The thermal vibration amplitude parameters from the multipole refinement were subjected to the rigid-bond test,[19] to check the deconvolution of the thermal vibration displacements from the valence electron density deformations. The test was satisfied very well for all bonds in the iron porphyrin moiety, with $|\Delta\langle u^2\rangle| < 0.001$ Å^2 along all bonds. The rigid-molecule test,[20] which is an extension of the rigid-bond test to include nonbonded interatomic vectors, was satisfied to the same degree, indicating that the porphinato iron group vibrates as a rigid body.

The atomic thermal vibration parameters were fitted by the rigid-body plus nonrigid-librating-group (TLS + Ω) model.[21] The calculations showed the main vibrations to be translational, with the major component approximately perpendicular to the porphinato ring plane. The nonrigidly attached phenyl groups undergo torsional oscillations around the C–C bonds linking the phenyl groups to the meso carbon atoms, with rms amplitudes of 5.5 (3) and 2.2 (8)° for the phenyl groups attached to C(5) and C(10), respectively. The dihedral angles between the phenyl groups and the porphinato plane are 83.5 and 65.9° at room temperature[7] and 79.7 and 63.4° in the present study. Thus, both phenyl groups are forced toward the plane of the porphinato ring when the crystal contracts on cooling.

Deformation Maps. $\rho_{X\text{-}X}$ deformation maps through each of the two independent pyrrole rings are given in Figure 6a,b, and the map averaged over both pyrrole rings assuming *mm* symmetry is shown in Figure 6c. As observed in previous studies, the overlap density is most pronounced in the C_β–C_β and C_α–C_m bonds, and the C_α–C_β and C_β–C_β peaks are centered outside the five-membered ring, indicating ring strain.

The deformation density in $FeON_1$, $FeON_2$, and FeN_1N_2 planes is shown in Figures 7 and 8. Unlike the maps of the intermediate-spin (FeTPP and FePc) and low-spin (CoTPP) complexes studied previously, in this high-spin complex no accumulation occurs around the Fe atom in the *xy* direction. Rather, excess

(17) Luger, P.; Buschmann, J. *Angew. Chem. Suppl.* **1983**, 537–542.
(18) Geise, H. J.; Adams, W. J.; Bartell, L. S. *Tetrahedron* **1969**, *25*, 3045–3052.
(19) Hirshfeld, F. L. *Acta Crystallogr., Sect. A: Cryst. Phys., Diffr., Theor. Gen. Crystallogr.* **1973**, *A29*, 239–244.
(20) Rosenfeld, R. E.; Trueblood, K. N.; Dunitz, J. D. *Acta Crystallogr., Sect. A: Cryst. Phys., Diffr., Theor. Gen. Crystallogr.* **1978**, *A34*, 828–829.
(21) Trueblood, K. N. *Acta Crystallogr., Sect. A: Cryst. Phys., Diffr., Theor. Gen. Crystallogr.* **1978**, *A34*, 950–954. Dunitz, J. D.; White, D. N. J. *Acta Crystallogr., Sect. A: Cryst. Phys., Diffr., Theor. Gen. Crystallogr.* **1973**, *A29*, 93–94. Schomaker, V.; Trueblood, K. N. *Acta Crystallogr., Sect. B: Struct. Crystallogr. Cryst. Chem.* **1968**, *B24*, 63–76.

Table VIII. Iron Atom d-Orbital Populations[a]

term symbol	$^5B_{2g}$	$^5A_{1g}$	$^5B_{1g}$	$^5E_{2g}$	exptl refinement III	exptl refinement IV	spherical
$d_{x^2-y^2}$	1 (16.7%)	1 (16.7%)	2 (33.3%)	1 (16.7%)	1.31 (22%)	1.42 (24%)	1.2 (20%)
d_{z^2}	1 (16.7%)	2 (33.3%)	1 (16.7%)	1 (16.7%)	0.88 (15%)	1.04 (17.5%)	1.2 (20%)
d_{xz}, d_{yz}	2 (33.3%)	2 (33.3%)	2 (33.3%)	3 (50%)	2.72 (46%)	2.52 (42.6%)	2.4 (40%)
d_{xy}	2 (33.3%)	1 (16.7%)	1 (16.7%)	1 (16.7%)	1.03 (17%)	0.93 (15.7%)	1.2 (20%)
total	6	6	6	6	5.95	5.92	6

[a] The standard deviation on the population parameters is between 0.06 and 0.08 e.

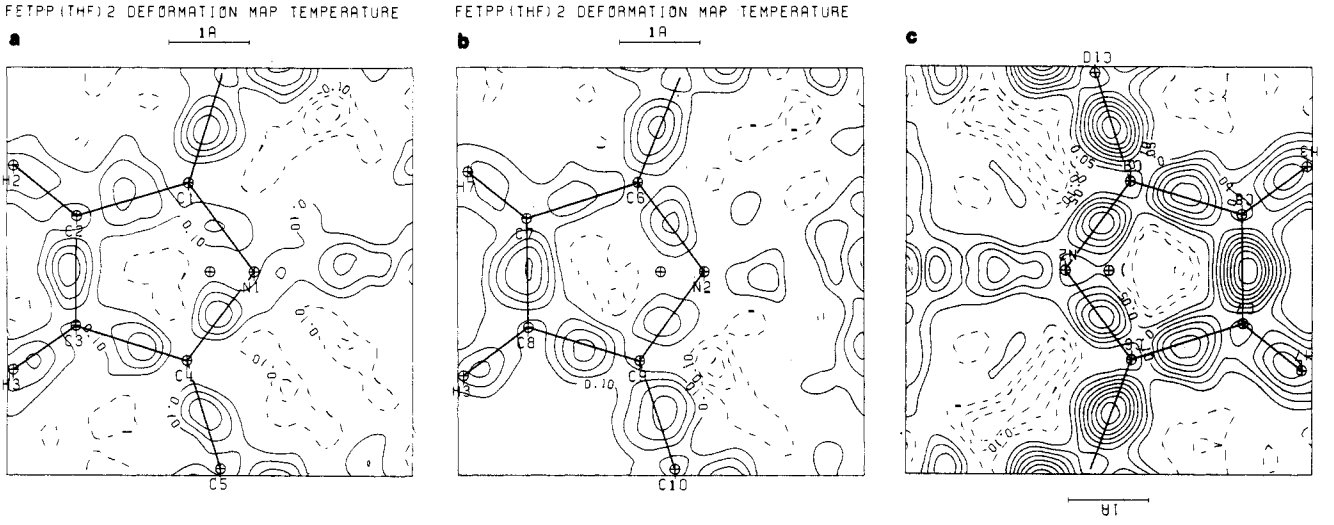

Figure 6. Deformation density in the pyrrole planes (a) of the N_1 pyrrole ring, (contours at 0.1 e Å^{-3}, negative contours broken, zero contour omitted); (b) of the N_2 pyrrole ring (contours as in (a)); (c) after averaging over the four half-rings (contours at 0.05 e Å^{-3}).

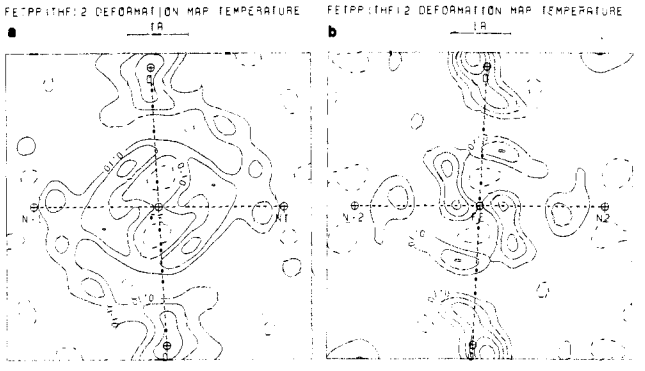

Figure 7. Deformation density in the Fe 2N 2O planes (contours as in Figure 6a): (a) plane containing N_1; (b) plane containing N_2.

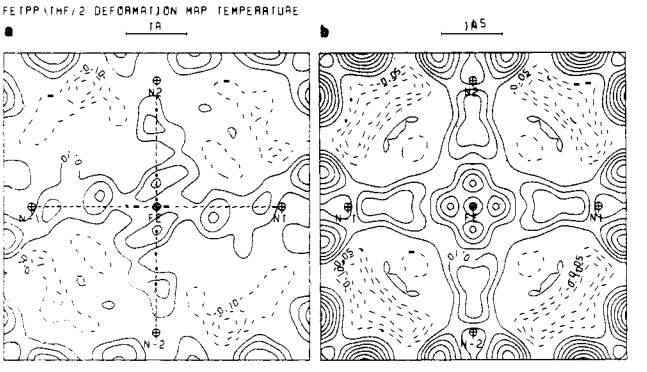

Figure 8. Deformation density in the Fe 4N plane: (a) before averaging, (contours as in Figure 6a); (b) after averaging over *mm* symmetry (contours as in Figure 6c).

density is observed in the Fe–N bonds (0.2 (1) e/Å^3 at 0.25 Å from the metal), which is interpreted as evidence for σ-donation from the porphyrin ligands. In the intermediate- and low-spin complexes this covalency effect leads to a nonzero population of the crystal field destabilized orbitals. Density accumulation is also observed out of plane in the *xz* and *yz* directons.

A choice between alternative ground-state configurations may be made on the basis of the electron density distribution. Several high-spin, quintet, ground states possible in D_{4h} symmetry are defined in Table VIII. They include $^5B_{2g}$, $^5A_{1g}$, $^5E_{2g}$, and $^5B_{1g}$. The lack of density accumulation in the *xy* and *z* directions is not compatible with either the $^5B_{2g}$ or the $^5A_{1g}$ state, but it supports $^5E_{2g}$ or $^5B_{1g}$, both of which have only one electron in the d_{xy} orbital. However, the latter state has two electrons in the $d_{x^2-y^2}$ orbital, which seems unlikely for a ground-state configuration.

Analysis of the Multipole Refinements. As expected for a high-spin state, the populations of the higher (i.e. $l > 0$) multipoles on the iron atom, which describe deviations from spherical symmetry, are small, though above the limit of statistical significance. The value of the Mössbauer quadrupole splitting, derived from the experimental d-orbital populations and the charges on nitrogen and oxygen atoms, is 0.6 (3) mm/s, compared with the spectroscopic value of −2.57 mm/s at 128 K.[7,8] The comparison is affected by the need to use a Sternheimer antishielding factor to convert the X-ray results to the equivalent spectroscopic values. Values of $R = 0.22$ and $\gamma = -10$ were used.[22]

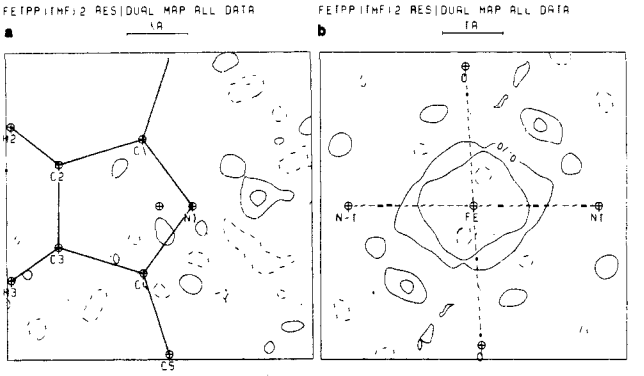

Figure 9. Residual maps (contours as in Figure 6a): (a) in the plane of one of the pyrrole rings; (b) in the Fe 2N 2O plane.

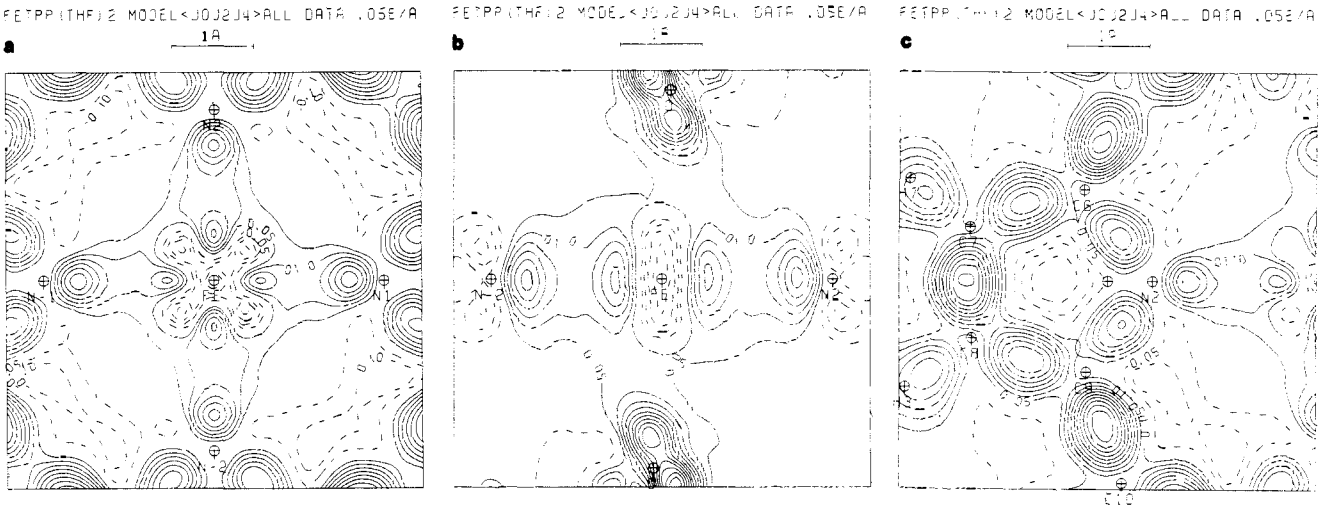

Figure 10. Model maps from refinement 1V (contours as in Figure 6c): (a) in the Fe 4N plane; (b) in a Fe 2N 2O plane; (c) in the plane of the pyrrole ring.

The Mössbauer results of Boso et al.[8] are interpreted in terms of a spherically symmetric d^5 subshell, plus a sixth electron in a prolate d_{z^2} orbital, which is oriented along a pseudotrigonal axis defined by one Fe–O bond and two Fe–N bonds. There is no evidence for such a trigonal distortion of the electron density in the results presented here. The distribution around the iron atom is close to spherical, the main distortion being represented by the multipole parameter P_{44+}, which places density along the Fe–N bonds. This accumulation is attributed to covalency of the metal–ligand interaction and is also found in theoretical deformation maps on the $Fe^{III}(H_2O)_6$ ion.[23]

The net charge on the iron atom is found to be +0.80 e. This is in accordance with a σ-donation from the ligands to the iron atom and in good agreement with values found in the study of FeTPP (+0.82 e) in which identical (HF) scattering factors were used. The nitrogen atoms bear a negative charge (–0.43 e), as do the oxygen atoms of the THF ligand (–0.37 e). The total charge on the THF ligand is negative (–0.77 e), a possible indication of π-back-donation to the THF molecule. For comparison, the charge on the axial methoxy ligand in Fe^{III}TPPOMe was found to be –0.6 e. The carbon atoms of the phenyl group are positively charged, with an average charge of +0.2 e.

Table VII lists the multipole parameters obtained in this study. For the porphyrin ring atoms, they are generally similar to those obtained in the earlier studies of CoTPP and FeTPPOMe, as may be expected given the almost invariant appearance of the pyrrole plane deformation maps. Significantly populated multipoles are (C_α) P_{33+}, (C_β) P_{20}, P_{33+} and P_{33-}, (C_m) P_{20} and P_{33+}, ($C_{\phi 1}$) P_{20} and P_{33+}, and ($C_{\phi 2}$) P_{20} and P_{33+} for all complexes. the local coordinate systems of the N and C_m atoms were selected differently for FeTPP; for the other atoms the agreement with the present results is good.

The residual maps obtained after the multipole refinement (Figure 9a,b) show the multipole fit to be excellent in the porphyrin macrocycle, but a diffuse shell of residual density is observed around the Fe atom (Figure 9b), suggesting insufficient flexibility in the Fe radial function.

The model deformation density in the plane of the pyrrole ring (Figure 10a, refinement IV) shows features in the C–C bonds and the nitrogen lonepair that are more pronounced than those in the experimental deformation map. This suggests that even the high-order parameters used in the calculation of the experimental deformation map are somewhat biased by the spherical-atom assumption. A second cause of the sharper image achieved in the model maps is the inclusion of the model-calculated amplitudes of all reflections up to $(\sin\theta)/\lambda = 1$ Å^{-1}, even those too weak to be measured.

The asphericity of the iron atom is clearly reproduced by the model (Figure 10). A depletion of electron density is observed along the z axis, in accordance with the low population of the d_{z^2} orbital.

As described elsewhere[24] d-orbital occupancies of the metal atom can be derived from the multipole parameters, assuming that the overlap density and the asphericity of any 4p orbital density are small. The results are compared with the populations of the iron quintet states in Table VIII.

The less-than-spherical-atom populations of both the d_{z^2} and d_{xy} orbitals are compatible with the $^5B_{1g}$ and $^5E_{2g}$ states but not with the other alternatives. The populations of the $d_{x^2-y^2}$ and the $d_{xz,yz}$ orbitals are almost intermediate between those of $^5B_{1g}$ and $^5E_{2g}$, in particular when the final refinement (IV) is considered. However, since the iron states with which comparison is made are ionic states, they do not account for covalency effects that will increase the $d_{x^2-y^2}$ population through σ-donation and to a lesser extent decrease the $d_{xz,yz}$ population through π-acceptance. Our previous studies show the effect of σ-donation to be quite large (0.6 electrons in CoTPP, about 0.4 electrons in FeTPP); it easily accounts for the observed excess density in $d_{x^2-y^2}$ above that predicted for $^5E_{2g}$. Thus, the multipole analysis leads to the same conclusion derived qualitatively from the examination of the deformation density maps, i.e., that the $^5E_{2g}$ state is the main contributor to the ground state of the complex.

Discussion. A further analysis of the electron distribution determined in this study and the corresponding ground-state assignment requires comparison with parallel theoretical calculations. No such calculations are available as yet for $Fe^{II}(THF)_2TPP$. The most extensive theoretical study of a six-coordinate Fe(II) complex was done on diammine(porphinato)iron(II), $Fe^{II}(NH_3)_2P$.[25] This calculation includes quintet, triplet, and singlet states and accounts for part of the correlation energy through configuration interaction. Though the geometry selected is rather different, the in-plane and axial iron–ligand distances being smaller than in $FeTPP(THF)_2$, the calculation puts ^5E as "clearly" the lowest state. It is concluded that the character of the ^5E state is largely Fe(III) $e_g\pi^*$, one electron being transferred from the iron atom to the π-system of the porphyrin ring. Such a conclusion does not contradict the present experimental results. The d-electron populations $d_{xy}^{0.93}$, $d_{xz,yz}^{2.52}$, $d_{z^2}^{0.88}$, and $d_{x^2-y^2}^{1.42}$ indicate the $d_{xz,yz}$ orbitals to be populated by about 0.5 electron less than predicted for the ^5E configuration and thus are compatible with significant back-donation into the π^*-orbitals as proposed.

(22) Finklea, S.; Cathey, L.; Amma, E. L. *Acta Crystallogr., Sect. A: Cryst. Phys., Diffr., Theor. Gen. Crystallogr.* **1976**, *A32*, 529.
(23) Koritsanszky, T.; Coppens, P.; Newton, M. D., unpublished results.
(24) Holladay, A.; Leung, P.; Coppens, P. *Acta Crystallogr., Sect. A: Cryst. Phys., Diffr., Theor. Gen. Crystallogr.* **1983**, *A39*, 377–387.
(25) Rawlings, D. C.; Gouterman, M.; Davidson, E. R.; Feller, D. *Int. J. Quant. Chem.* **1985**, *28*, 797–822.

A more detailed comparison between experiment and theory will require an advanced theoretical calculation on $Fe^{II}(THF)_2TPP$ itself. It is clear that such a calculation is a challenge, even with the best computers available at present.

The temperature dependence of the Fe–O and Fe–N distances and the increase in magnetic moment below 60 K suggest that the ground state may be a function of temperature. However, the relative constancy of the Mössbauer results seems to rule out large changes in the electron distribution around the iron atom. We are presently making EXAFS measurements to examine the variability of the iron coordination sphere below liquid-nitrogen temperature.

Acknowledgment. Support of this work by the National Institutes of Health (Grants HL2388404 to P. Coppens and GM34073 and AM19856 to R. H. Blessing) and the National Science Foundation (Grant CHE8403428) is gratefully acknowledged.

Registry No. $Fe^{II}(THF)_2TPP$, 29189-60-4.

Supplementary Material Available: Listings of coefficients of least-squares planes, deviations from planes, and dihedral angles (4 pages); listing of observed and calculated structure factors (40 pages). Ordering information is given on any current masthead page.

Bis-Benzimidazole-Appended Binucleating Porphyrin Ligands: Synthesis, Characterization, and X-ray Structure

Nigel G. Larsen, Peter D. W. Boyd,[1] Steven J. Rodgers, Gerald E. Wuenschell, Carol A. Koch, Susan Rasmussen, John R. Tate, Brian S. Erler, and Christopher A. Reed*

Contribution from the Departments of Chemistry, University of Southern California, Los Angeles, California, 90089-1062, and University of Auckland, Auckland, New Zealand.
Received March 28, 1986

Abstract: The synthesis and characterization of some new binucleating tetraarylporphyrin ligands is reported. The potentially most useful example is α,α,5,15-bis[*N*-(2-methylbenzimidazolyl)acetamidophenyl]-α,α,10,20-bis(pivalamidophenyl)porphine (**8**). The ligands have two appended benzimidazole arms which are designed to chelate a second metal directly above the porphyrin. The synthetic methodology for obtaining both the 5,15 (i.e., trans) and the 5,10 (i.e., cis) bis-appended ligand from an $\alpha, \alpha, \alpha, \alpha$,5,10,15,20 *tetra*-functionalized starting material is described in detail. A key design feature of the ligand system is amenability to single-crystal X-ray structure determination and this is demonstrated with an X-ray structure of a copper(II) complex. Crystal data for $CuC_{74}H_{66}N_{12}O_4 \cdot 1.5$(diethyl ether)·toluene are the following: monoclinic, $C2/c$, a = 31.240 (4) Å, b = 16.769 (5) Å, c = 35.199 (4) Å, β = 121.4 (1)°; R = 0.0823, R_w = 0.0826. H bonding between the benzimidazole moieties and the pivalamido pickets is seen to determine the structural disposition of the appendages lying above the porphyrin ring. Iron(III) porphyrin complexes of these new ligands exist in a hydroxo monomer form as well as the familiar μ-oxo dimer form.

In the last decade the synthetic model approach to hemoprotein structure and reactivity has developed into a sophisticated art and a detailed science. Synthetic elaboration at the periphery of a tetrapyrrolic core has provided porphyrins with a wide array of useful appendages and superstructures. The aesthetic appeal of these structures has been captured in their nomenclature with descriptive terms such as cyclophane,[2] picket-fence,[3] chelated,[4] capped,[5] strapped,[6] basket-handle,[7] tail,[8,9] hanging base,[10] crowned,[11] bridged,[12] double,[13] pocket,[14,15] face-to-face,[16,17] cofacial,[18] strati,[19] gable,[20] caroteno,[21] tulip garden,[22] and lipid[23] porphyrins. A particular emphasis in the more recent work has been the construction of *binucleating* porphyrins which hold a pair of metals in close proximity.[11,16-20,24-33] Part of the motivation for this synthesis has been to model the structure[27,31,34,35] or the reactivity[36-38] of cytochrome oxidase[39] whose heterobinuclear heme/copper active site functions as nature's oxygen electrode. The rate and efficiency of cytochrome oxidase catalysis in the four-electron reduction of oxygen to water has proved to be very difficult to duplicate in man-made systems. A number of synthetically elegant porphyrins having appended ligands for binding a second metal have been reported, but a convincing structural model for the active site of cytochrome oxidase has yet to be characterized. The evolution of the model compound approach toward this goal requires first and foremost the unambiguous establishment of structure in binuclear systems. This essentially means single-crystal X-ray structure determination since the

* University of Southern California.

(1) University of Auckland.
(2) Diekmann, H.; Chang, C. K.; Traylor, T. G. *J. Am. Chem. Soc.* **1971**, *93*, 4068-4070. Traylor, T. G.; Tsuchiya, S.; Campbell, D.; Mitchell, M.; Stynes, D.; Koga, N. *J. Am. Chem. Soc.* **1985**, *107*, 604-614.
(3) Collman, J. P.; Gagne, R. R.; Reed, C. A.; Halbert, T. R.; Lang, G.; Robinson, W. T. *J. Am. Chem. Soc.* **1975**, *97*, 1427-1439.
(4) Chang, C. K.; Traylor, T. G. *Proc. Natl. Acad. Sci. U.S.A.* **1973**, *70*, 2647-2650. Geibel, J.; Cannon, J.; Campbell, D.; Traylor, T. G. *J. Am. Chem. Soc.* **1978**, *100*, 3575-3585.
(5) Almog, J.; Baldwin, J. E.; Crossley, M. J.; Debernardis, J. F.; Dyer, R. L.; Peters, M. K. *Tetrahedron* **1981**, *37*, 3589-3606.
(6) Baldwin, J. E.; Crossley, M. J.; Klose, T.; O'Rear, E. A., III; Peters, M. K. *Tetrahedron* **1981**, *38*, 27-39.
(7) Momenteau, M.; Loock, B.; Mispelter, J.; Bisagni, E. *Nouv. J. Chim.* **1979**, *3*, 77-79. Lavalette, D.; Tetreau, C.; Mispelter, J.; Momenteau, M.; Lhoste, J.-M. *Eur. J. Biochem.* **1984**, *145*, 555-565.
(8) Mashiko, T.; Reed, C. A.; Haller, K. J.; Kastner, M. E.; Scheidt, W. R. *J. Am. Chem. Soc.* **1981**, *103*, 5758-5767.
(9) Collman, J. P.; Brauman, J. I.; Doxsee, K. M.; Halbert, T. R.; Bunnenberg, E.; Linder, R. E.; LaMar, G. N.; Del Gaudio, J.; Lang, G.; Spartalian, K. *J. Am. Chem. Soc.* **1980**, *102*, 4182-4192.
(10) Momenteau, M.; Lavalette, D. *J. Chem. Soc., Chem. Commun.* **1982**, 341-343.
(11) Chang, C. K. *J. Am. Chem. Soc.* **1977**, *99*, 2819-2822.
(12) Battersby, A. R.; Buckley, D. G.; Hartley, S. G.; Turnball, M. D. *J. Chem. Soc., Chem. Commun.* **1976**, 879-881.
(13) Ogoshi, H.; Sugimoto, H.; Yoshida, Z. *Tetrahedron Lett.* **1977**, 169-172.

0002-7863/86/1508-6950$01.50/0